Nanoscale

ROYAL SOCIETY OF CHEMISTRY

COMMUNICATION

View Article Online
View Journal | View Issue

Cite this: *Nanoscale*, 2023, **15**, 470

Received 29th September 2022,
Accepted 6th December 2022

DOI: 10.1039/d2nr05404c

rsc.li/nanoscale

DNA conformational equilibrium enables continuous changing of curvatures†

Dake Mao, Victoria E. Paluzzi, Cuizheng Zhang and Chengde Mao *

Assembly of complex structures from a small set of tiles is a common theme in biology. For example, many copies of identical proteins make up polyhedron-shaped, viral capsids and tubulin can make long microtubules. This inspired the development of tile-based DNA self-assembly for nanoconstruction, particularly for structures with high symmetries. In the final structure, each type of motif will adopt the same conformation, either rigid or with defined flexibility. For structures that have no symmetry, their assembly remains a challenge from a small set of tiles. To meet this challenge, algorithmic self-assembly has been explored driven by computational science, but it is not clear how to implement this approach to one-dimensional (1D) structures. Here, we have demonstrated that a constant shift of a conformational equilibrium could allow 1D structures to evolve. As shown by atomic force microscopy imaging, one type of DNA tile successfully assembled into DNA spirals and concentric circles, which became less and less curved from the structure's center outward. This work points to a new direction for tile-based DNA assembly.

DNA has been exploited to build nanostructures and nanomachines by programmed self-assembly.[1–6] A key event of structural DNA nanotechnology is the development of a series of rigid DNA nanomotifs,[7–10] which must satisfy various, precise geometric requirements. In contrast, structural flexibility in nanomotifs would lead to uncontrolled association among motifs; and thus, is generally avoided. Consequently, all nanomotifs will have the same, predefined conformation in the final structure. This is a powerful strategy but fails in assembling continuously changing structures. For example, spirals are simple structures, topologically equivalent to 1D chains, and could, in principle, be assembled from tiles in a 1D sense. In the spiral, individual tiles will have similar, but different conformations. Tiles become less and less curved from the structure's center outward. Strategies and nanomotifs reported previously could not be easily adapted to assemble such continuously changing structures.[11–15] Thus, we ask a question: can we design an assembly strategy/nanomotif in such a way that the tiles accommodate the necessary flexibility to continuously change their curvature? Would these assemble into structures that require the tiles to adapt to continuously changing conformations? Herein, we have developed an approach to address this problem. As a demonstration, a series of DNA spirals have been assembled by homo-polymerization of single component, 21-nucleotide (nt)-long DNA strands. The structures have been thoroughly characterized by polyacrylamide gel electrophoresis (PAGE) and atomic force microscopy (AFM) imaging.

Fig. 1 illustrates the DNA assembly route. Each DNA architecture is homo-polymerized from a two-stranded, double-crossover (DX)-like (DXL) motif, which, in turn, is assembled *via* homodimerization from a short, single DNA strand. The basic sequence **h** is 20 nucleotides (nts) long and all other strands, **hX**s, contain a chemical group X (a single base A, G, T, C, or two bases AA, or a fluorescein, Fig. S1†) at the 3′ end in addition to the basic sequence **h**. These strands are named according to the chemical group X as **hX**. Strand **h** includes four palindromic segments: two 6-nt-long segments in the middle and two 4-nt-long segments at the two ends. During the polymerization, two **h** strands will first hybridize and associate with each other by the two central 6-nt-long palindromes to form a DXL motif. The four remaining palindromic tails could further hybridize with each other, resulting in one-dimensional (1D) arrays, exhibiting a well-defined straight morphology (Fig. 1a). The 1D arrays could be viewed as two, long, interconnected, parallel, pseudo-continuous DNA duplexes. For strands **hX**s, the extra chemical groups (X) will fundamentally change the array morphologies (Fig. 1b). X will remain un-paired and can either be out of the duplex as a spare group or stack in the helical domains. The two conformations consist of a dynamic and reversible equilibrium. Its balance is determined by the chemical structure of X and the

Purdue University, Department of Chemistry, West Lafayette, IN 47907, USA. E-mail: mao@purdue.edu

† Electronic supplementary information (ESI) available. See DOI: https://doi.org/10.1039/d2nr05404c

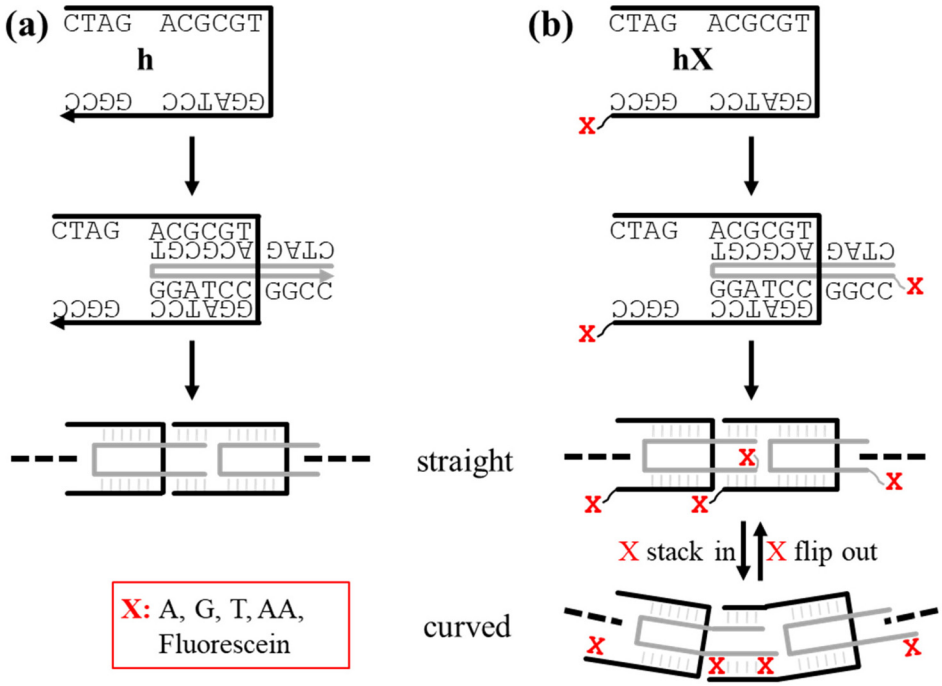

Fig. 1 DNA homopolymerization. (a) Assembly from tiles with one defined conformation. Two copies of the DNA strand **h** consisting of four palindromes can dimerize and further homopolymerize to 1D arrays. (b) Assembly from tiles under conformational equilibrium. The DNA strand **hX** has an extra chemical group X. When stacking into DNA duplexes, X will cause 1D arrays to bend because of the length difference between the duplexes at the top and bottom. When X flips out of the helical domain, the 1D arrays will be straight. By different combinations of the two conformational states, the 1D arrays could continuously change their curvatures in a wide range.

system's environment. When X is out of the duplex domain, the resulting 1D arrays have a straight morphology. When X stacks in the duplex, the two parallel duplexes will have different lengths and the mismatched lengths will force the 1D arrays to bend into curved shapes.[16,17] For purines (G or A) and fluorescein, X has a large aromatic plane, and thus, can stack strongly with DNA base pairs. For pyrimidine (T and C), X has a small aromatic plane; thus it can only weakly stack with DNA base pairs and is more likely to remain outside of the DNA duplex.[18] Overall, the existence of X will have two effects: (1) 1D arrays can bend because of the length mismatch; (2) the bending extent along the 1D array could widely vary as the conformational equilibrium of the motifs could be easily changed. In the DNA ladder, the equilibrium is also influenced by the surrounding environment, for example, the bending angle could decrease and the circular structure could be more straight by more X base flipping out.

We first investigated DNA assembly in solution by native PAGE. DNA was dissolved in TAE/Mg^{2+} buffer and directly analyzed with native PAGE at room temperature after thermal annealing. At 20 μM (Fig. S2†), strand **h** assembled into large polymers, which appeared as a band near the well. In contrast, DNA strands (**hX**) with extra chemical groups appeared as smears with increased electrophoretic mobilities, indicating that they are smaller polymers. This observation suggested that the sticky-end cohesion was weakened by the extra chemical group intercalation. This caused the DNA polymer to dissociate into oligomers in solution. Judging by the native PAGE data, the destabilizing capability of X followed this order: C < G < A ≪ T ~ AA ~ F. At 2 μM, no appreciable polymerization in native PAGE was observed for all DNA strands except **h** (Fig. S3†).

Then we used AFM to directly visualize the morphology of the assembled DNA 1D arrays. DNA solutions in TAE/Mg^{2+} buffer were deposited on the freshly cleaved mica surface and incubated for 10 min. After removing the excess solution, a TA/Mg^{2+}/Ni^{2+} imaging buffer was added onto the mica surface and the DNA samples were imaged in tapping mode.[19,20]

DNA samples from every individual DNA strand (**h** or **hX**) assembled into large nanostructures, which exhibited a rich variety of morphologies depending on the identity of the chemical group (X) and the DNA concentration (Fig. 2 and S4†). Poly(**h**), the polymer assembled from strand **h** without any extra chemical group at the 3′ end, appeared as straight fibers. Poly(**hC**) behaved similarly, indicating that the extra base (C) at the 3′ end flipped outside of the helical domain. When X is the chemical group (A, G, T, AA, and fluorescein) other than C, the assembled polymers showed obvious, but different degrees of curvature. At a low DNA concentration (0.5 μM), well-separated, discrete circles or arcs were observed. The circles of poly(**hAA**) and poly(**hF**) were substantially smaller than the circles of poly(**hA**) and poly(**hG**), and they all were smaller than poly(**hT**) circles. At a high DNA concentration (2 μM), closely packed spirals or multi-layered, con-

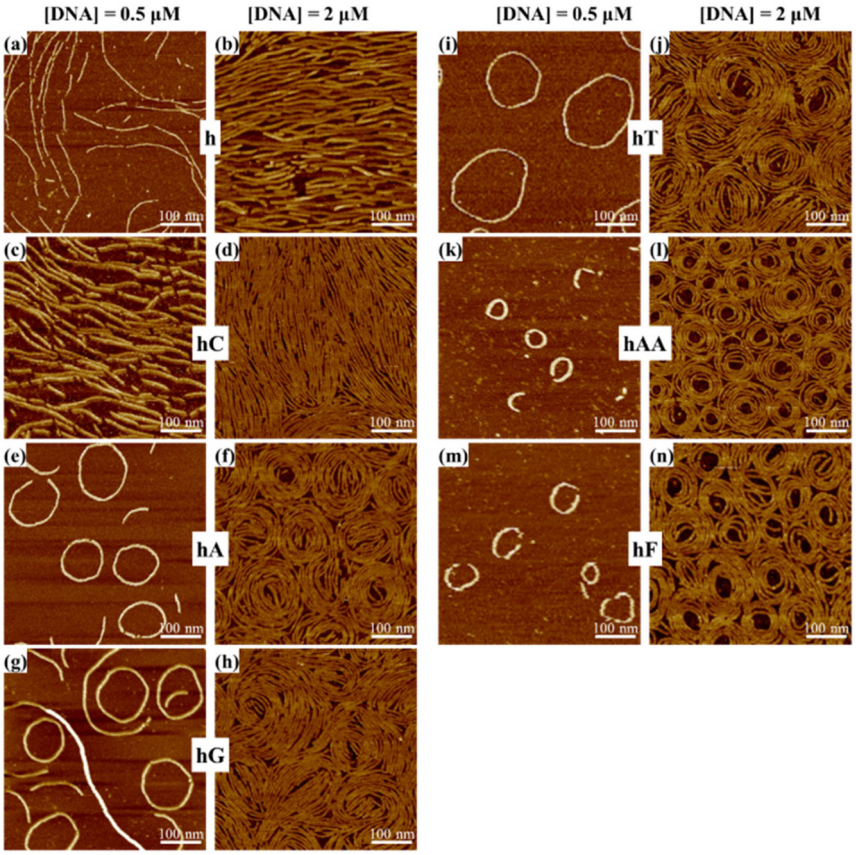

Fig. 2 AFM study of the morphologies of DNA homopolymers assembled from different DNA strands at two different DNA concentrations. (a) & (b) h; (c) & (d) hC; (e) & (f) hA; (g) & (h) hG; (i) & (j) hT; (k) & (l) hAA; and (m) & (n) hF.

centric circles completely covered the mica surfaces. The Mg^{2+} concentration had a similar effect on the DNA assembly as the DNA concentration did (Fig. S5†). Divalent cations Mg^{2+} could promote the homopolymerization and DNA adsorption onto the mica surface, thus increasing the effective DNA concentration on the mica surface for DNA assembly. Please note that the two exact DNA concentrations (0.5 and 2 μM) were chosen from our experience based on the strength of the inter-motif interaction (sticky-end interaction). For different sticky-ends (in terms of length and base composition), the interaction strength would vary and the DNA concentration would be adjusted accordingly. But the overall phenomenon should be similar.

To understand the driving force of the flexible bending in the homopolymer, we measured the average bending angle between two adjacent DXL motifs for all curved homopolymers (Fig. 3). In a closed DNA homopolymer circle, the sum of all the bending angles ($\boldsymbol{\theta}$) was 360°. The number of DXL motifs in the circle could be calculated by the circle contour length ($\boldsymbol{L}$) divided by the motif length ($\boldsymbol{d}$), which is 10 base pairs, or 3.3 nm assuming the rise of a DNA duplex is 0.33 nm/base pair. Thus, the bending angle ($\boldsymbol{\theta}$) could be calculated as:

$$\boldsymbol{\theta} = 360°/(\boldsymbol{L}/\boldsymbol{d}) = 360°/(\boldsymbol{L}/3.3\ \text{nm})$$

By tuning the incubation conditions, we prepared poly(**hX**) as single circles for all curved designs and imaged them by AFM (Fig. S6–S10†). Note that no conformational constraints were imposed on inter-motif interactions during the cyclization of the single circles. We used TopoStats,[21] an imaging processing software, to filter AFM images and measure contour lengths of the circles (Fig. 3b, ESI†). For **hT**, the average bending angle between motifs was 2.42 ± 0.37°, while the angles for **hA** and **hG** were 3.35 ± 0.60° and 3.56 ± 3.81°, respectively. This phenomenon occurs because purines have a larger aromatic plane than pyrimidines, and thus can more effectively stack into a DNA duplex and cause the array to bend. For **hAA**, the bending angle further increased to 5.14 ± 1.22° due to the insertion of two bases (compared with one base) into a duplex which would introduce a larger length mismatch (Fig. 1b). Interestingly, the bending effect was not limited to natural DNA bases. Other chemical moieties with a flat, aromatic plane could stack into the DNA duplex and induce arrays to bend as well.[22,23] When a fluorescein unit was incorporated at the 3′ end (strand **hF**), an average bending angle of 4.28 ± 1.01° was observed.

We further conducted kinetic studies to understand the effects of inter-motif flexibility and assembly conditions on the final morphologies of the DNA homopolymers (Fig. 4 and S11–

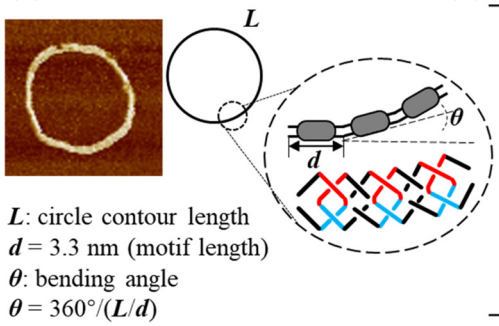

(b)

X	L (nm)	θ (°)
h	N.A.	N.A.
hC	N.A.	N.A.
hA	365 ± 67	3.35 ± 0.60
hG	437 ± 178	3.56 ± 3.81
hT	503 ± 76	2.42 ± 0.37
hAA	249 ± 83	5.14 ± 1.22
hF	298 ± 95	4.28 ± 1.01

Fig. 3 The bending angle of the curved DNA structure with different modifications. (a) Schematic drawing of bending angle calculation from single closed circles. (b) The calculated bending angles of motifs from different DNA strands.

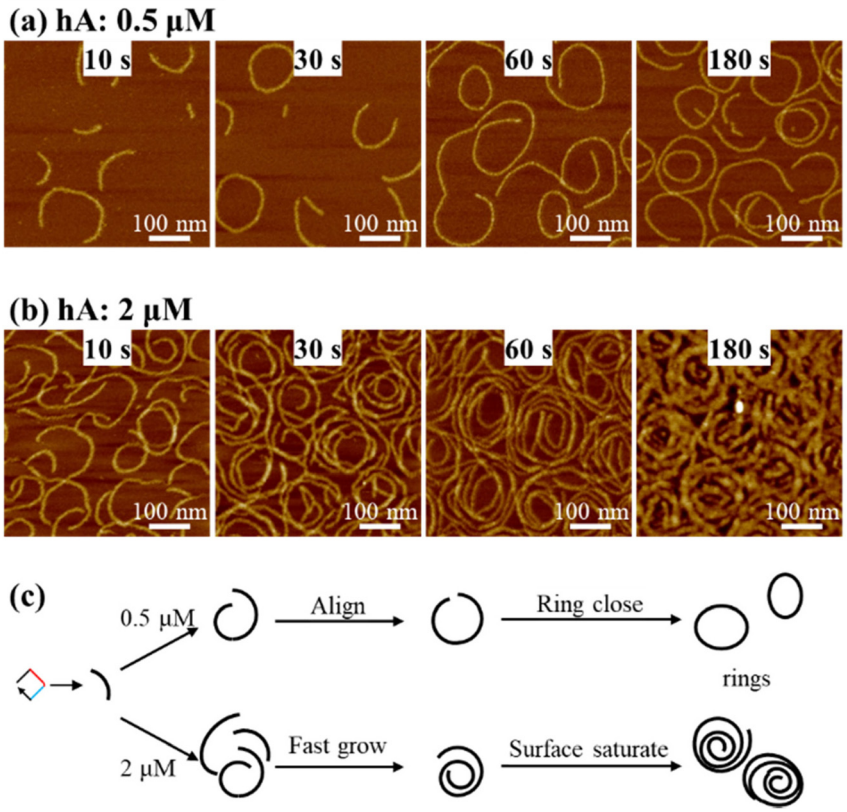

Fig. 4 The assembly kinetics of curved structures at different DNA concentrations exemplified by **hA**. AFM images of curved structure formation at DNA concentrations of (a) 0.5 μM and (b) 2 μM and (c) proposed schemes of assembly under thermodynamic or kinetic control.

S16†). To capture intermediate states at specific time-points during assembly, DNA samples were rapidly dried and immediately AFM imaged in air. Such a protocol prevented the DNA samples from any further change that could be associated with aqueous AFM imaging. At a high DNA concentration (2.0 μM), **hX** molecules quickly adsorbed onto the mica surface and grew fast, continuous 1D arrays adjacent to existing 1D arrays (Fig. 4a), which initially formed single rings and long arcs at 10 s and then transformed spirals or concentric ring structures after 30 s. At a low DNA concentration (0.5 μM), DNA molecules slowly adsorbed onto the mica surface and more distinct circles formed (Fig. 4b). At this concentration, the DNA ladder formed single rings at 30 s and further grew into ~50% single rings and ~50% two-layer concentric rings, indicating the continuous DNA deposition. Generally, the DNA molecules adsorbed onto the mica surface and oligomerized on the substrate with surface templating, and simultaneously self-aligned or joined with other oligomers. The final mor-

phology was determined by the kinetic competition between adsorption (thus the effective surface DNA concentration) and refiguration (circle-closing alignment) (Fig. 4c). For the slow adsorption at a low DNA concentration, the homopolymer had sufficient time to align itself in an intra-polymer fashion into a closed circle. The random stacking in/flipping out of X rendered a range of circle size distribution. In contrast, the fast adsorption at a high DNA concentration saturated the surface. Thus, a large number of polymers would simultaneously form and align in an inter-polymer fashion to form concentric rings or continuous spirals to maximize coverage of the mica surface. The flexibility of X stacking in/flipping out allowed the motifs gain flexibility to adopt the necessary curvature to form the final morphologies. According to native PAGE (Fig. S2†), the sticky ends were weaker for **hT**, **hAA** and **hF**. This explained the slow growth rate of the corresponding DNA homopolymers (Fig. S14–S16†). Furthermore, inter-motif assembly is a function of DNA concentration. Thus, the formation of circular structures took a longer time at a 0.5 μM DNA concentration than at a 2 μM DNA concentration. However, if the incubation was through the thermodynamically slow annealing process with a high DNA concentration, the final morphology turned into only concentric circles. This demonstrated that the circle-closing alignment would minimize the system's free energy (Fig. S17†). With the inflexible chemical groups, only the semi-straight fibers' density change was observed during the changes in time and DNA concentration.

In summary, this study provides a novel and straightforward strategy to introduce dynamic flexibility to DNA homopolymers and bend the DNA nanostructures by a chemical modification (natural bases or other aromatic moieties) at the ends of DNA strands. This dynamic bending allows for the assembly of DNA nanostructures with constantly changing curvatures from single component strands. Such capability was not accessible previously and could be achieved by a large number of DNA components.[16,24,25] This study has expanded the toolbox for structural DNA nanotechnology in two aspects. In large and complicated nanostructures, such as DNA origami, the extra base could be applied to weaken the connection strength or to fine tune the partial curvature. Additionally, this strategy could enable the flexible and multiple curvature in DNA tile-based design with limited DNA components. Conceivably, the dynamic flexibility of DNA homopolymers enables their use as soft or elastic building units for nanomachines and nanorobots.[26–32]

Conflicts of interest

There are no conflicts to declare.

Acknowledgements

We thank NSF (CMMI 2025187 and CCF 2107393) for financial support of this work.

References

1 N. C. Seeman and H. F. Sleiman, DNA nanotechnology, *Nat. Rev. Mater.*, 2017, **3**, 17068.
2 C. G. Evans and E. Winfree, Physical principles for DNA tile self-assembly, *Chem. Soc. Rev.*, 2017, **46**, 3808–3829.
3 M. R. Jones, N. C. Seeman and C. A. Mirkin, Programmable materials and the nature of the DNA bond, *Science*, 2015, **347**, 1260901.
4 A. V. Pinheiro, D. Han, W. M. Shih and H. Yan, Challenges and opportunities for structural DNA nanotechnology, *Nat. Nanotechnol.*, 2011, **6**, 763–772.
5 F. Zhang, J. Nangreave, Y. Liu and H. Yan, Structural DNA nanotechnology: State of the art and future perspective, *J. Am. Chem. Soc.*, 2014, **136**, 11198–11211.
6 Q. Hu, H. Li, L. Wang, H. Gu and C. Fan, DNA Nanotechnology-Enabled Drug Delivery Systems, *Chem. Rev.*, 2019, **119**, 6459–6506.
7 E. Winfree, F. Liu, L. A. Wenzler and N. C. Seeman, Design and self-assembly of two-dimensional DNA crystals, *Nature*, 1998, **394**, 539–544.
8 P. W. K. Rothemund, Folding DNA to create nanoscale shapes and patterns, *Nature*, 2006, **440**, 297–302.
9 Y. Ke, L. L. Ong, W. M. Shih and P. Yin, Three-dimensional structures self-assembled from DNA bricks, *Science*, 2012, **338**, 1177–1183.
10 M. Zheng, Z. Li, L. Liu, M. Li, V. E. Paluzzi, J. H. Choi and C. Mao, Kinetic DNA Self-Assembly: Simultaneously Co-folding Complementary DNA Strands into Identical Nanostructures, *J. Am. Chem. Soc.*, 2021, **143**, 20363–20367.
11 C. E. Castro, H. J. Su, A. E. Marras, L. Zhou and J. Johnson, Mechanical design of DNA nanostructures, *Nanoscale*, 2015, **7**, 5913–5921.
12 Y. Yang, J. Wang, H. Shigematsu, W. Xu, W. M. Shih, J. E. Rothman and C. Lin, Self-assembly of size-controlled liposomes on DNA nanotemplates, *Nat. Chem.*, 2016, **8**, 476–483.
13 H. G. Franquelim, A. Khmelinskaia, J. P. Sobczak, H. Dietz and P. Schwille, Membrane sculpting by curved DNA origami scaffolds, *Nat. Commun.*, 2018, **9**, 811.
14 C. G. Evans and E. Winfree, Physical principles for DNA tile self-assembly, *Chem. Soc. Rev.*, 2017, **46**, 3808–3829.
15 S. Lee, S. Park, M. T. Raza, T. B. N. Nguyen, T. H. N. Vu, A. Tandon and S. H. Park, Multirule-Combined Algorithmic Assembly Demonstrated by DNA Tiles, *ACS Appl. Polym. Mater.*, 2022, **4**, 5441–5448.
16 H. Dietz, S. M. Douglas and W. M. Shih, Folding DNA into twisted and curved nanoscale shapes, *Science*, 2009, **325**, 725–730.
17 M. Zheng, Q. Li, Q. Li, V. E. Paluzzi, J. H. Choi and C. Mao, Engineering the Nanoscaled Morphologies of Linear DNA Homopolymers, *Macromol. Rapid Commun.*, 2021, **42**, 2100217.
18 R. E. Holmlin, P. J. Dandliker and J. K. Barton, Charge Transfer through the DNA Base Stack, *Angew. Chem., Int. Ed. Engl.*, 1997, **36**, 2714–2730.

19 M. Bezanilla, B. Drake, E. Nudler, M. Kashlev, P. K. Hansma and H. G. Hansma, Motion and enzymatic degradation of DNA in the atomic force microscope, *Biophys. J.*, 1994, **67**, 2454–2459.
20 L. Liu, Y. Li, Y. Wang, J. Zheng and C. Mao, Regulating DNA Self-assembly by DNA–Surface Interactions, *ChemBioChem*, 2017, **18**, 2404–2407.
21 J. G. Beton, R. Moorehead, L. Helfmann, R. Gray, B. W. Hoogenboom, A. P. Joseph, M. Topf and A. L. B. Pyne, TopoStats – A program for automated tracing of biomolecules from AFM images, *Methods*, 2021, **193**, 68–79.
22 X. D. Liu, H. Y. Diao and N. Nishi, Applied chemistry of natural DNA, *Chem. Soc. Rev.*, 2008, **37**, 2745–2757.
23 A. Ruiz-Carretero, P. G. A. Janssen, A. Kaeser and A. P. H. J. Schenning, DNA-templated assembly of dyes and extended π-conjugated systems, *Chem. Commun.*, 2011, **47**, 4340–4347.
24 D. Han, S. Pal, J. Nangreave, Z. Deng, Y. Liu and H. Yan, DNA origami with complex curvatures in three-dimensional space, *Science*, 2011, **332**, 342–346.
25 K. Pan, D. N. Kim, F. Zhang, M. R. Adendorff, H. Yan and M. Bathe, Lattice-free prediction of three-dimensional structure of programmed DNA assemblies, *Nat. Commun.*, 2014, **5**, 5578.
26 J. Bath and A. J. Turberfield, DNA nanomachines, *Nat. Nanotechnol.*, 2007, **2**, 275–284.
27 H. Liu and D. Liu, DNA nanomachines and their functional evolution, *Chem. Commun.*, 2009, 2625–2636.
28 J. Li, C. Fan, H. Pei, J. Shi and Q. Huang, Smart drug delivery nanocarriers with self-assembled DNA nanostructures, *Adv. Mater.*, 2013, **25**, 4386–4396.
29 H. Joh and D. E. Fan, Materials and Schemes of Multimodal Reconfigurable Micro/Nanomachines and Robots: Review and Perspective, *Adv. Mater.*, 2021, **33**, 2101965.
30 J. B. Lee, S. Peng, D. Yang, Y. H. Roh, H. Funabashi, N. Park, E. J. Rice, L. Chen, R. Long, M. Wu and D. Luo, A mechanical metamaterial made from a DNA hydrogel, *Nat. Nanotechnol.*, 2012, **7**, 816–820.
31 S. Hamada, K. G. Yancey, Y. Pardo, M. Gan, M. Vanatta, D. An, Y. Hu, T. L. Derrien, R. Ruiz, P. Liu, J. Sabin and D. Luo, Dynamic DNA material with emergent locomotion behavior powered by artificial metabolism, *Sci. Robot.*, 2019, **4**, eaaw3512.
32 Y. Guo, Q. Zhang, Q. Zhu, J. Gao, X. Zhu, H. Yu, Y. Li and C. Zhang, Copackaging photosensitizer and PD-L1 siRNA in a nucleic acid nanogel for synergistic cancer photoimmunotherapy, *Sci. Adv.*, 2022, **8**, eabn2941.